



Deeply Supervised Skin Lesions Diagnosis with Stage and Branch Attention

Wei Dai^a, Rui Liu^a, Tianyi Wu^a, Min Wang^a, Jianqin Yin^b, Jun Liu^{a,c,*}

^a City University of Hong Kong, Hong Kong, China

^b Beijing University of Posts and Telecommunications, Beijing, China

^c Shenzhen Research Institute, City University of Hong Kong, Shenzhen, China

ARTICLE INFO

Article history:

Received xx June 2022

Received in final form xx xx 2022

Accepted xx xx 2022

Available online xx xx 2022

Communicated by xxx xxx

Keywords:

Skin lesions classification

Deep supervision

Stage attention

Branch attention

Vision transformer

ABSTRACT

Accurate and unbiased examinations of skin lesions are critical for the early diagnosis and treatment of skin diseases. Visual features of skin lesions vary significantly because the images are collected from patients with different lesion colours and morphologies by using dissimilar imaging equipment. Recent studies have reported that ensembled convolutional neural networks (CNNs) are practical to classify the images for early diagnosis of skin disorders. However, the practical use of these ensembled CNNs is limited as these networks are heavyweight and inadequate for processing contextual information. Although lightweight networks (e.g., MobileNetV3 and EfficientNet) were developed to achieve parameters reduction for implementing deep neural networks on mobile devices, insufficient depth of feature representation restricts the performance. To address the existing limitations, we develop a new lite and effective neural network, namely HierAttn. The HierAttn applies a novel deep supervision strategy to learn the local and global features by using multi-stage and multi-branch attention mechanisms with only one training loss. The efficacy of HierAttn was evaluated by using the dermoscopy images dataset ISIC2019 and smartphone photos dataset PAD-UFES-20 (PAD2020). The experimental results show that HierAttn achieves the best accuracy and area under the curve (AUC) among the state-of-the-art lightweight networks. The code is available at <https://github.com/anthonyweidai/HierAttn>.

© 2022 Elsevier B. V. All rights reserved.

1. Introduction

Skin conditions and disorders are among the most common human diseases to affect millions of people (Guy Jr et al., 2015a,b). Statistical data shows that around 20% of Americans are diagnosed with malign cutaneous diseases (Esteva et al., 2017). Skin cancer, consisting of non-melanoma and melanoma, affected more than 1.5 million new cases globally in 2020. Skin cancer is estimated to be the fifth most common detected cancer in the U.S., with 196,060 new cases reported in 2021 (Sung et al., 2021). The annual cost for treatment of skin

cancer is projected to triple from 2011 to 2030 (Guy Jr et al., 2015b). Proactive detection and early diagnosis are critically essential to save patients. For instance, the five-year survival rate for melanoma patients could be 99% with early-stage diagnosis and treatment, whereas the survival rate is dropped to around 27% if the conditions are detected in the late stage (Sung et al., 2021).

Traditional methods for detecting skin disorders include skin cancer screening by self-examination and clinical examination. Among these methods, self-examination is the most common method for the early detection of skin diseases. Around 53% of patients with melanomas are self-examined before approaching medical experts (Avilés-Izquierdo et al., 2016). Clinical skin examination can provide affirmative screening of skin cancers

*Corresponding author.

e-mail: jun.liu@cityu.edu.hk (Jun Liu)

arXiv:2205.04326v6 [eess.IV] 23 Aug 2022

with a high detection accuracy (Loescher *et al.*, 2013). However, clinical examinations consume a considerable amount of time for medical professionals to review a large number of dermoscopic images. The long waiting time of weeks or months could delay the treatment and result in unexpected progress of the skin conditions.

The advances in imaging technology make it possible to diagnose skin lesions by analysing optical images of the skin lesions. The imaging modalities in skin examination include reflectance confocal microscopy, total body photography, teledermatology, and dermoscopy. Among all the imaging modalities, dermoscopy is a non-invasive imaging method without reflecting light to examine the skin lesions with up to 10× magnification (Loescher *et al.*, 2013). However, manual analysis of dermoscopic images is time-consuming, and the examination results are subjective to healthcare providers.

Due to the sophisticated features of skin lesion images, it is nontrivial to automatically detect unhealthy skin areas with satisfactory accuracy. Previously, computer-aided approaches were proposed to analyse skin lesion images. Histogram thresholding employs empirical thresholds to isolate lesions from the rest of the skin tissues (Celebi *et al.*, 2009). Principle component analysis (PCA) for colour histogram was further utilised in lesion colour space clustering for segmentation (Perruch *et al.*, 2013). Gradient vector flow was computed to extract the smoothness and compactness of curve shapes in skin lesions for separating lesions from neighbouring tissues (Zhou *et al.*, 2011). However, the majority of these techniques require heavy human participation and cannot extricate sufficient features from a whole skin lesion image to diagnose skin diseases.

To achieve an accurate and unbiased diagnosis of skin diseases, deep learning has been applied to extract representative features and provide an end-to-end analysis of medical images. A multi-scale and two-stream convolutional neural network (CNN) was introduced in skin lesions classification (Kawahara and Hamarneh, 2016). Moreover, the classification activation feature map was used to capture region of interest information for learning indicative lesion representations (Tang *et al.*, 2020). Modified ResNet with U-shape CNN architectures were also applied to the classification and segmentation of skin lesions (Chen *et al.*, 2018; Xie *et al.*, 2020). In other studies, researchers processed three modalities of patient data, including non-image metadata, clinical and dermoscopy images, in a two-stage feature fusion network to enhance skin lesions classification performance (Tang *et al.*, 2022). To learn a different degree of contextual information, Dai *et al.* introduced an encoder which resizes features in different scales (Dai *et al.*, 2022). To improve the diagnostic results, researchers assembled several models, such as ResNeXt, NASNet, SENet, DenseNet121 and EfficientNet, to detect skin cancer, and the highest accuracy of these models was reported up to 94.2% and 92.6% on the ISIC2018 and ISIC2019 datasets, respectively (Adegun and Viriri, 2021). However, the majority of reported networks, especially those constructed by combining several models, consumed a large number of computational resources and were highly time-consuming due to the increased complexity of models.

Recently, lightweight algorithms have been reported to promote the use of deep learning in conducting direct skin cancer screening with limited computational resources in clinical computers and mobile devices. One major solution to achieving lightweight CNNs is the depthwise separable convolution (DWSCConv), which replaces the standard convolution with depthwise convolution within one channel and pointwise convolution along each channel for the depletion of learnable parameters (Howard *et al.*, 2017). As for lightweight vision transformer (ViT) networks, sparse attention (Pan *et al.*, 2022), random feature attention (Suwanwimolkul and Komorita, 2022), and low-rank approximation (Yang *et al.*, 2022) were adopted to reduce ViTs' size and computational cost. Most recently, several models leveraged CNN and ViT by applying standard convolution (Pan *et al.*, 2022) or DWSCConv (Mehta and Rastegari, 2021) to downsize tensors before each ViT module. Moreover, knowledge distillation was applied to reduce model parameters (Song *et al.*, 2022). Although the aforementioned techniques have attained satisfactory results in common object recognition, lightweight deep learning models have not been investigated for skin lesions analysis.

This article aims to address the challenges in balancing the reliability and accuracy of skin lesion analysis with small memory storage and minimal computational cost. The major novelty and key contributions of this study are:

- We introduce a new lightweight and deeply supervised architecture with diverse attention mechanisms, namely HierAttn, to distinguish multi-class skin lesions. HierAttn achieves the top-level performance with a smaller size than other competing mobile models for both the ISIC2019 and PAD2020 datasets.
- We develop a novel deep supervision method, branch attention algorithm, to learn both local and global representations from coarse level to fine level of features with hierarchical pooling and aggregate the extracted hierarchical features by tensors assembling. Since the hierarchical pooling and tensor assembling do not introduce additional learnable parameters, high-level features generated by the stage attention block can be extracted without increasing the model size. Moreover, branch attention does not introduce additional loss computation, which is computation-friendly compared to the conventional deep supervision method with multiple losses.
- We propose the same channel attention (SCAttn) module based on global averaging pooling without unnecessary modification of channel-wise features. The SCAttn design effectively extracts global features and outperforms other attention methods like squeeze and excitation while avoiding the increment of the model parameters to keep a small model size.
- We propose the stage attention block, consisting of a

SCAttn block followed by a convolution-transformer hybrid (CTH) block, to thoroughly learn the regional and global high-level feature representations. As shown in Fig. 1, the HierAttn network involves a novel CTH block by adding a skip connection and stochastic depth to gain optimal performance.

We review related literature in Sec. 2 and explain the proposed methodology in Sec. 3. We present and discuss the experiment results in Sec. 4 and Sec. 5. We summarise the major findings in Sec. 6.

2. Related Work

2.1. CNNs in skin lesions diagnosis

The recent advances in machine learning have introduced an increasing number of deep neural networks. The deep learning models, including InceptionV3, VGG, EfficientNet, ResNet, DenseNet, etc., have been applied to classify skin lesions (Esteve et al., 2017; Weng et al., 2020; Gessert et al., 2020). Moreover, the models, assembling several networks (e.g., ResNeXt, NASNet, SENet, DenseNet121, and EfficientNet) in several streams or stages, were utilised in skin lesions classification (Gessert et al., 2020; Mahbod et al., 2020; Attique Khan et al., 2021). The ISIC2019 challenge winner applied an ensemble model accumulating EfficientNet B0 to B6, SENet154, and two ResNeXt to achieve a 92.6% average classification accuracy; however, the model is comparatively large with more than 100 M parameters, making it impractical for clinical and home use (Gessert et al., 2020).

2.2. Deeply supervised learning

Adding and widening layers are common methods to improve training metrics by increasing the learning parameters of networks. However, both methods increase the computational complexity and requirements of hardware during training. Deeply supervised learning is frequently used to learn coarse-to-fine features from intermediate branches. Instead of adding layers to the network, deep supervision usually uses auxiliary supervision branches in critical intermediate stages during training (Wang et al., 2015). Multilevel losses are widely used in deep supervision to extract feature information from stages to improve the model's performance. For instance, GoogleNet has three losses in three branches, separately (Szegedy et al., 2015). Liu et al. applied deep supervision with multiple losses to improve object edges learning (Liu and Lew, 2016). However, the features in various stages are fed into simple tensor operations separately. They do not have a direct correlation influence on each other.

2.3. Attention mechanisms

The attention mechanism is a biomimetic cognitive method used in diverse computer vision assignments such as image classification (Woo et al., 2018; Hu et al., 2018; Dosovitskiy et al., 2020; Hou et al., 2021; Mehta and Rastegari, 2021) and image segmentation (Mehta and Rastegari, 2021; He et al., 2022). An example of the attention network is the SENet, which obtains global representations by global average pooling and channel-wise feature response by squeeze and excitation (Hu et al., 2018). The convolution block attention module (CBAM) improves the SENet by using a larger kernel size to encode spatial information (Woo et al., 2018). Coordinated attention fur-

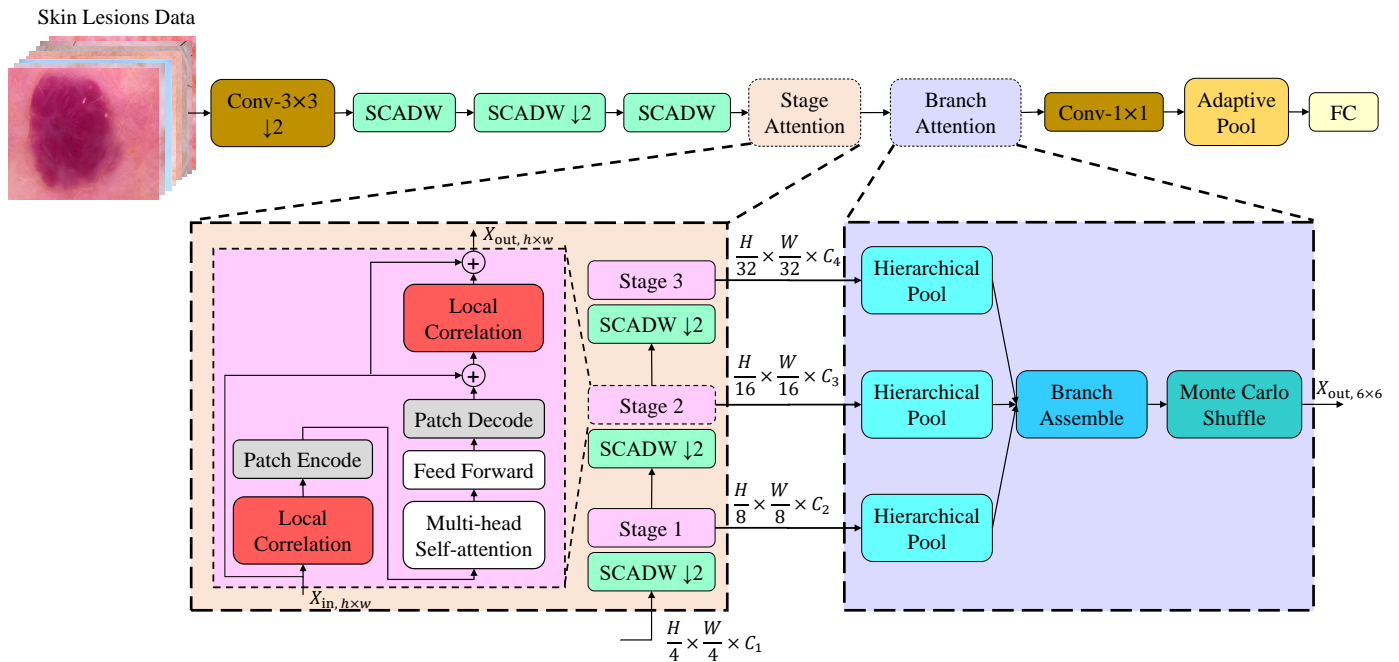


Fig. 1: **HierAttn architecture.** Conv- $n \times n$ represents a standard convolution, and SCADW refers to a depthwise separable convolution block with the SCAttn module. Down-sampling blocks are marked with $\downarrow 2$. Stage attention has a SCADW block followed by a CTH block (pink block) that thoroughly aggregates local features and learns contextual representations. Branch attention utilises hierarchical pooling to extract global and local features steadily.

ther advances the global average pooling by encoding channel relationships and long-range dependencies via average pooling along different axes (Hou et al., 2021). However, they introduce more learnable parameters and consume more computational resources than the SENet.

2.4. Vision transformer

To improve the computational efficiency and meet the scalability requirement, self-attention mechanisms, particularly transformers, are introduced into computer vision from natural language processing. With self-attention, a ViT replaces the traditional convolution method with a transformer encoder (Dosovitskiy et al., 2020). Because the input images are directly split into patches and embedded, the ViT models are still very large, with more than 100 M parameters (Dosovitskiy et al., 2020). The standard transformer has been applied to process sequences of image patches to learn the inter-patch representations. However, the original transformer method ignores the inductive biases (e.g., translation equivariance and locality) inherent to CNNs, which leads to poor performance when training with insufficient data (Dosovitskiy et al., 2020). Recently, ViT was utilised in skin lesions evaluation by appending a ViT branch to CNN-based U-shape architecture for improving long-range dependencies and contextual information extraction, but an additional branch notably increased the model weight (Wu et al., 2022).

2.5. Lightweight networks

To reduce computational cost and model weight, researchers proposed several well-accepted methods such as knowledge distillation, DWSCConv, and efficient self-attention design. Although knowledge distillation can effectively reduce learnable parameters, it bears the huge computational cost of the training process. Moreover, complex teacher and student network structures and parameters updated between the two networks should be carefully designed (Reiß et al., 2021). In addition, based on DWSCConv method, MobileNetV2, MobileNetV3, EfficientNet, MnasNet, and ShuffleNet were constructed and obtained relatively satisfactory performance (Sandler et al., 2018; Zhang et al., 2018; Tan and Le, 2019; Tan et al., 2019; Howard et al., 2019). To reduce the latency of splitting images, computer scientists from Apple proposed MobileViT to tackle the loss of inductive biases by taking convolution and transformer to form a hybrid block (Mehta and Rastegari, 2021). However, it can not entirely learn representations because the number of its layers is deficient. Moreover, to the best of our knowledge, the aforementioned networks have not been applied to skin lesion analysis, and their performance remains unknown.

3. Proposed Methodology

3.1. Skin lesion dataset

Two publicly available skin lesions datasets, ISIC2019 (Tschandl et al., 2018; Adegun and Viriri, 2021; Combalia et al., 2019) and PAD2020 (Pacheco et al., 2020), are used in this research for development and evaluation of the proposed

methods. Dermoscopy and smartphones are two standard methods to capture skin lesions images. Thus, the two datasets effectively represent current image data for the classification of skin lesions. The data distribution of the two datasets is shown in Fig. 2.

ISIC2019 dataset consists of 25,331 dermoscopy images with eight categories: actinic keratosis (ACK), basal cell carcinoma (BCC), benign keratosis (BKL), dermatofibroma (DF), melanoma (MEL), melanocytic nevus (NV), squamous cell carcinoma (SCC), vascular lesion (VASC). Three of them (ACK, BCC and SCC) belong to the non-melanoma skin cancer. Melanoma is the most severe skin cancer that is caused by uncontrolled growing cells that can produce pigment. The vascular lesions (VASC) can be either benign or malign and requires close monitoring over a period of time. The remaining categories of skin lesions are benign conditions. The PAD2020 dataset includes 2,298 skin lesion images with six classes: ACK, BCC, BKL, MEL, NV, and SCC, collected by using smartphones. Compared to ISIC2019, PAD2020 has two fewer classes, DF and VASC, because of lacking photos of skin lesions.

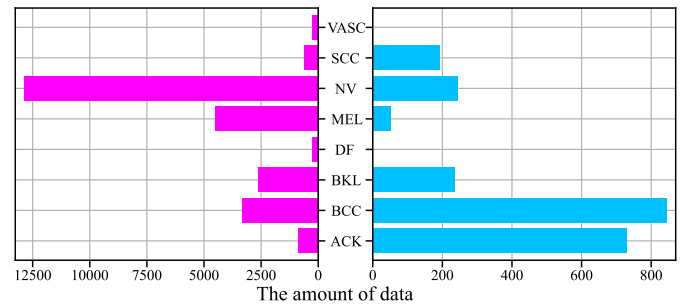


Fig. 2: **Data distribution** on ISIC2019 (left image) and PAD2020 (right image)

3.2. Pre-processing

3.2.1. Image pre-processing

The data among different classes from the ISIC2019 dataset has a large black area [see Fig. 3 (a)], which damages the evaluation performance of deep learning models. Thus, an adaptive cropping method is taken to identify and crop these images. The original image is first turned into greyscale [Fig. 3 (b)] and then binarised an adaptive threshold ranging from 50 to 255 [Fig. 3 (c)]. After that, the contour of the binarised image is detected to confirm the circle location. When the value of the circle area divided by the whole image area is between 0.01 and 0.9, the region enclosed by the circle is cropped and saved [Fig. 3 (d)].

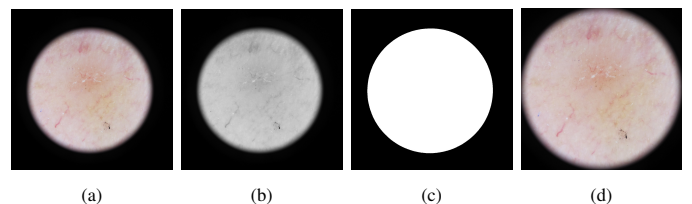


Fig. 3: **The progress in cropping image** (a) original image, (b) greyed image, (c) binarised image, and (d) cropped image.

3.2.2. Data balance

In this study, an imbalance ratio is defined to assess the imbalance problem quantitatively. The imbalance ratio is a fraction of the number of images of the majority class over the minority class. The imbalance ratio for ISIC2019 and PAD2020 are 53.9 and 16.3, respectively. Such relatively high imbalance ratios can remarkably reduce the performance of training, according to previous research (Buda et al., 2018). The data imbalance could lead to a low validation result for the minor class, though the averaged validation metrics over all classes could be high. Data balance by oversampling or undersampling for each class is a practical technique to handle the dataset with a huge imbalance ratio. Oversampling and undersampling are simultaneously utilised to balance ISIC2019 and PAD2020 data. After sampling, 2500 images and 500 images are collected for each class in the ISIC2019 and PAD2020 datasets, respectively. Thus, the amount of data after balancing totals 20000 and 3000 on ISIC2019 and PAD2020, respectively, is close to the total amount of unbalanced data.

Oversampling uses horizontal flips, random crops, Gaussian blur, linear contrast, random translation, rotation, and shear on a small scale to generate new images from the old images. As for undersampling, the random selection of a fixed number of images tends to have a class-overlapping problem. Thus, we apply an adaptive data analysis method called instance hardness (IH) to alleviate this adverse effect. Instance hardness is defined as:

$$\text{IH}_{\mathcal{L}}((x_i, y_i)) = 1 - \frac{1}{|\mathcal{L}|} \sum_{j=1}^{|\mathcal{L}|} p(y_j|x_i, g_j(t, \alpha)) \quad (1)$$

where \mathcal{L} is a prior with non-zero probability while treating all other learning algorithms as having zero probability, g is a machine learning algorithm trained on t with the hyperparameter α , and y_j is the label for data x_i .

Outliers and mislabelled data are expected to have high IH. Thus, IH analysis was applied in undersampling to remove those data with a high IH. This research uses the random forest as the machine learning method g , referenced from the imbalanced-learn study (Smith et al., 2014; Lemaître et al., 2017).

3.3. HierAttn architecture

The paper introduces an efficient and lite Convolution-Transformer model [see Fig. 1], HierAttn, for skin lesions diagnosis. The main idea of this model is to hierarchically learn the local and global representations by utilising various attention mechanisms. Branch attention allows the network to extract various levels of features from different layers. Moreover, the SCAttn module in our new HierAttn network leverages the DWSCConv by supplementing global information to improve performance. The three novel mechanisms (i.e., SCAttn, stage attention, and branch attention) consume miniature parameters or no learnable parameter, which results in the tiny size of HierAttn. Besides, the stage attention utilises an effective self-attention hybridising convolution to keep inductive biases and reduce the latency, inspired by the MobileViT architecture (Mehta and Rastegari, 2021). The attention modules

are described in the following sections. Detailed structures of HierAttn are shown in Table 1.

3.3.1. Branch attention

Zhang et al. employed a contrastive loss to improve the feature interactions during training among different intermediate stages (Zhang et al., 2022). Instead, we propose a novel deep supervision method, brach attention (i.e., lower right in Fig. 1), utilising hierarchical pooling to downsize tensors from different stages, tensors assembling to improve the interactions of the downsized features and learn the hierarchy of features from the assembled tensors. Moreover, by keeping the different sizes of pooling results, hierarchical pooling learns the local representations of tensors, generating large tensor size ($C \times 5 \times 5$), and attains tensors' global representations, generating small tensor size ($C \times 1 \times 1$). Additionally, the medium output tensor with size $C \times 3 \times 3$ is also designed as a buffer layer to keep both local and global features. The pooled tensors from different branches are then channel-wisely assembled. After that, the ensembled tensors are pixel-wisely assembled. At the end of branch attention, the pixel-wisely assembled tensors are pixel-wisely shuffled by utilising the Monte Carlo method. The branch attention is applied as a particular learning stage after each stage attention block (critical learning stage). Most importantly, by using such a practical design, branch attention does not introduce additional loss, which cost less computational cost than the conventional deep supervision method. The branch attention progress is illustrated in Fig. 4.

3.3.2. Same channel attention

The block modifies the DWSCConv with the SCAttn technique and results in a new block structure called SCADW block (i.e., green blocks in Fig. 1). Squeeze and excitation attention (SEAttn) blocks were proposed to enhance the expressive power of the learned features after depthwise convolution in the MobileNetV3 block (Howard et al., 2019). However, the pointwise convolution already extracts the channel-wise information, which suggests that the excitation of SEAttn is likely a redundant operation. Therefore, the SCAttn is introduced after depthwise convolution by global average pooling while maintaining the same number of learnable parameters as the DWSConv block. The SCAttn block is illustrated in Fig. 5.

3.3.3. Stage attention

Each stage attention module (i.e., lower left in Fig. 1) has a SCADW block with a stride of 2 followed by a convolution-transformer hybrid block. We apply the convolutions and transformers simultaneously to learn the local and global representations of an input skin lesion image with fewer parameters. The convolution-transformer hybrid (CTH) block (i.e., pink blocks in Fig. 1) utilised consecutive modules to process feature maps before and after encoding. The CTH block consists of a multi-head self-attention (MHSA) followed by a multilayer perceptron feed forward (FFN) layer, which is regarded as vision transformer (ViT). ViT learns long-range spatial dependence among encoded patches, which is shown in Fig. 6 (a). To integrate local features, local correlation through standard convolution is applied before and after the ViT module in the CTH

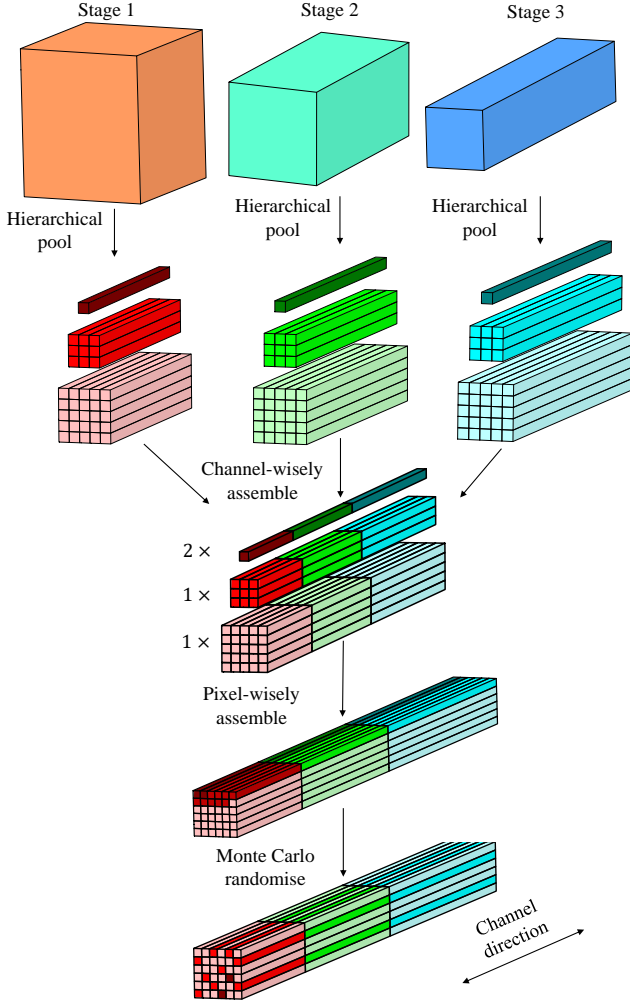


Fig. 4: Branch attention by hierarchical pooling, assembling and randomising tensors from different branches.

block, which is illustrated by Fig. 6 (b). Furthermore, we also add a skip connection to link the input and output of the CTH block. Stage attention module thoroughly rearranges feature maps by downsizing feature maps, and the CTH block further extracts the processed features. Thus, each stage attention module is regarded as a **critical learning stage** in HierAttn. The CTH block bottleneck can be formulated as:

$$\begin{aligned}
 X &= \text{LocalCorr}(X_{\text{in}}) + X_{\text{in}} \\
 Y &= \text{MHSA}(\text{Encode}(X)) \\
 Z &= \text{Decode}(\text{LayerNorm}(\text{FFN}(Y))) \\
 X_{\text{out}} &= \text{LocalCorr}(Z + X_{\text{in}}) + X_{\text{in}}
 \end{aligned} \quad (2)$$

3.3.4. Small-scale attention modules

SCAttn leverages SEAttn by keeping single-pixel attention through global averaging pooling and avoiding the modification of tensors along channel direction. It contributes to utilising an attention mechanism to extract global features after depth-wise convolution without introducing any learnable parameters. Moreover, branch attention does not increase model size because hierarchical pooling and tensor assembling in branch at-

tention are parameter-free. In addition, transformer operations lose spatial bias, increasing computational costs with a wider and deeper design to learn visual representations (Mehta and Rastegari, 2021). Therefore, ViT-Base, ViT-Large, and ViT-Huge models use the number of transformer blocks $L = 12, 24, 32$ and the number of embedded dimensions $d = 768, 1024, 1280$, respectively (Dosovitskiy et al., 2020). However, our new HierAttn only requires $L = 2, 4, 3$ and $d = 96, 120, 144$. The number of parameters for the new HierAttn and other state-of-the-art (SOTA) networks is summarised in Table 2.

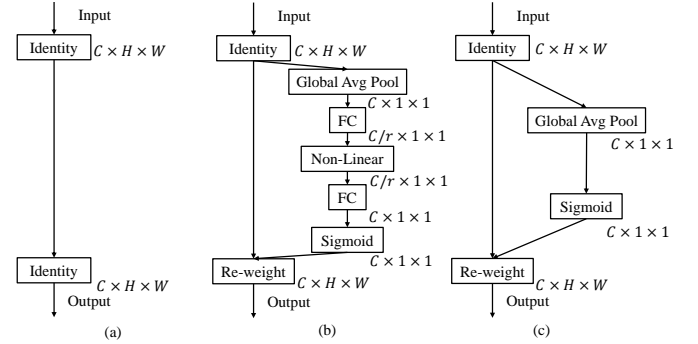


Fig. 5: Schematic comparison of the original block (without attention mechanism) (a), the SEAttn block (b), and the proposed SCAttn block (c).

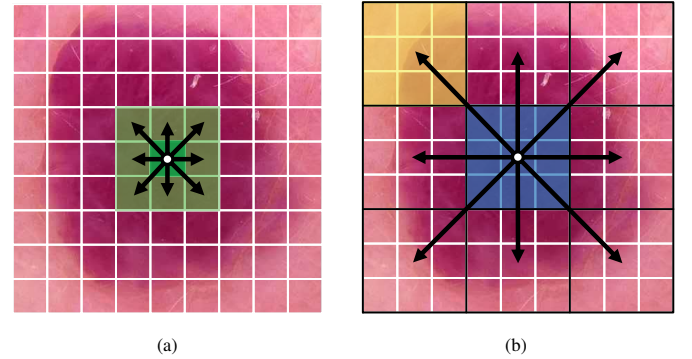


Fig. 6: Feature interactions in stage attention. (a) Local correlation extract local features and (b) Multi-head self-attention further learns global information.

4. Experimental Results

In this section, we first evaluate HierAttn performance on the ISIC2019 and PAD2020 datasets in Sec. 4.2. HierAttn delivers significantly better performance than the SOTA mobile networks (<6 M), which can be seen in Table 2 and Fig. 7. In Sec. 4.3, we conducted ablation studies for attention mechanisms in DWSCConv.

4.1. Evaluation metrics

The ISIC community recommends accuracy, ROC, and AUC to be the evaluation metrics for skin lesions classification (Cassidy et al., 2022). In our experiments, top-1 accuracy (abbrev. accuracy) is adopted to evaluate the performance of skin lesions classification (e.g., the proportion of correct values in inference

Table 1: **Detailed structures of the proposed HierAttn architecture.** Here, d means dimensionality of the input to the transformer layer in the CTH block. In the CTH block, kernel size is set as three and patch height and width are set as two.

Layer		Output size	Repeat	Output Channels	
				XS	S
Image		256×256			
Conv3 \times 3, \downarrow 2		128×128	1	16	16
SCADW			1	16	32
Conv3 \times 3, \downarrow 2		64×64	1	24	48
SCADW			2	24	48
Stage1	Conv3 \times 3, \downarrow 2 CTH block	32×32	1	48	64
			1	$48(d = 64)$	$64(d = 96)$
Stage1	Conv3 \times 3, \downarrow 2 CTH block	16×16	1	64	80
			1	$64(d = 80)$	$80(d = 120)$
Stage1	Conv3 \times 3, \downarrow 2 CTH block	8×8	1	80	96
			1	$80(d = 96)$	$96(d = 144)$
Branch attention		8×8	1	192	240
Conv1 \times 1			1	768	960
Pooling		1×1	1	8 or 6	8 or 6
Linear					
# Parameters				1.08 M	2.14 M

Table 2: **# Parameters and accuracy of different models.**

Model	# Parameters/M	Accuracy/%	
		IHSIC20000 \uparrow	IHPAD3000
MobileNetV2(Sandler et al., 2018)	2.23	93.45	87.44
MobileViT_s(Mehta and Rastegari, 2021)	4.94	94.72	88.22
MobileNetV3_Large(Howard et al., 2019)	4.21	94.77	88.78
ShuffleNetV2_1x(Zhang et al., 2018)	2.28	95.23	87.89
MnasNet1.0(Tan et al., 2019)	3.11	95.45	90.33
EfficientNet_b0(Tan and Le, 2019)	4.02	95.48	90.22
HierAttn_xs (ours)	1.08	96.15	90.11
HierAttn_s (ours)	2.14	96.70	91.22

results). Moreover, the receiver operating characteristic (ROC) curve and its area under the curve (AUC) are applied to demonstrate the more general performance of each model (e.g., the model’s robustness and scale invariance). Furthermore, each model’s number of parameters (# parameters) is applied to measure its weight.

4.2. Image classification on the skin lesions dataset

4.2.1. Implementation details

The HierAttn network and other SOTA lite models are trained and validated for 500 epochs on one RTX A4000 with a batch size of 64 images using AdamW optimiser (Loshchilov and Hutter, 2018) with 10-fold cross-validation and cross-entropy loss. The learning rate is ceased from 0.002 to 0.0002 during the first 30 epochs and then increased to 0.0002 utilising the cosine scheduler (Loshchilov and Hutter, 2017). L2 weight decay of 0.01 is adopted. Moreover, knowledge transfer is applied to reduce the training time and improve model performance. All transferred models for training in ISIC2019 were trained in ImageNet1K. The well-tuned models from ISIC2019 were then tuned in PAD2020. And the parameters of other layers of HierAttn after branch attention are randomly initialised.

Additionally, the transfer learning warm-up is applied to alleviate the negative influence of untransferred layers on transferred layers. On the first training 30 epochs, all transferred layers are frozen. After that, gradient calculation is required for all layers with learnable parameters. Furthermore, each model with 8 classes on ISIC2019 or 6 classes on PAD2020 has a similar number of parameters when two decimal places are kept. Thus, the number of parameters of each model is computed with eight classes to simplify the discussion. Meanwhile, mobile models with (1, 2.5) M, (2.5, 4) M, (4, 5.5) M parameters are regarded as "extra small", "small", and "medium", respectively.

4.2.2. Accuracy

Fig. 7 compares HierAttn with six other lightweight networks that are also trained on the ISIC2019 and PAD2020 datasets. Detailed values are illustrated in Table 2. Fig. 7 also demonstrates that HierAttn networks fall in the upper left region, which means they outperform other mobile architectures with relatively small sizes. For instance, with about 1.08 million parameters, HierAttn_s outperforms MobileNetV2 by 3.25%, MobileNetV3_large by 1.93%, ShuffleNetv2_1x by 1.47%, MnasNet1.0 by 1.25%, and EfficientNet-b0 by 0.55%

on the ISIC2019 validation set. Furthermore, HierAttn_s also outperforms MobileViT_s, which also contains convolution-transformer hybrid blocks, by 1.98% and 3.00% on ISIC2019 and PAD2020 datasets, respectively. Besides, HierAttn attains more than 90% accuracy on both the dermoscopy and the smartphone skin lesions image datasets, which demonstrates that HierAttn is versatile in visually diagnosing skin lesion images from various domains.

4.2.3. ROC and AUC

Fig. 8 illustrates that all models on experiments have more than 0.99 AUC on the ISIC2019 and 0.98 AUC on the PAD2020 validation sets, suggesting that they possess sufficient analytical capacities to conduct multi-classes lesions classification tasks. Furthermore, the ROCs of HierAttn_s and HierAttn_xs are the first and second closest to the point (0, 1) on both ISIC2019 and PAD2020 validation sets. Moreover, HierAttn_s and HierAttn_xs have the first and the second largest AUC on both datasets among all models, for instance, 0.99772 and 0.99558 on the ISIC2019 validation set, respectively. Thus, the ROCs

and AUCs show that HierAttn is the most reliable and superlative model to detect skin lesions among current conventional and advanced mobile models. Meanwhile, the same model's AUC of the PAD2020 validation set is lower than the ISIC2019 validation set, which means these models perform better on the ISIC2019 validation set (in conformity with Table 2).

4.3. Ablation studies

4.3.1. Implementation details

In ablation studies, the model used is HierAttn_s, and the dataset used is ISIC2019, if not mentioned. Other parameters are the same as Section 4.2.1.

4.3.2. Data balance methods

Fig. 9 elucidates the accuracy of different data balance methods on ISIC2019 and PAD2020. Firstly, the accuracy of IH (instance hardness) is higher than that of Rand (randomised sampling) on both datasets, which means IH can more effectively sample images than Rand. Secondly, IH exceeds 5.9%

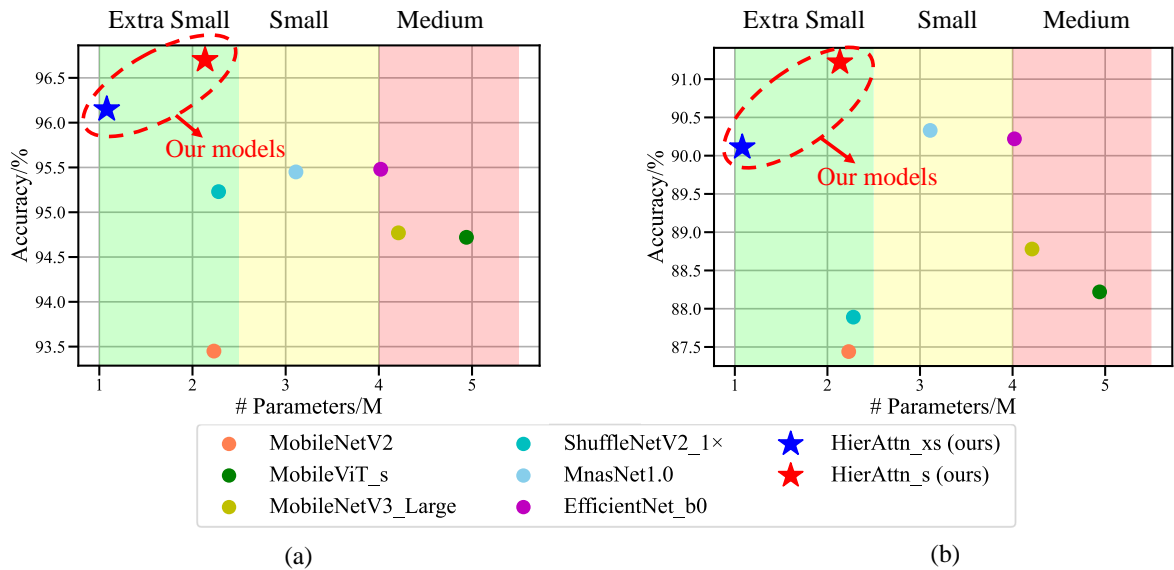


Fig. 7: HierAttn vs. SOTA models on (a) ISIC2019 and (b) PAD2020 validation set.

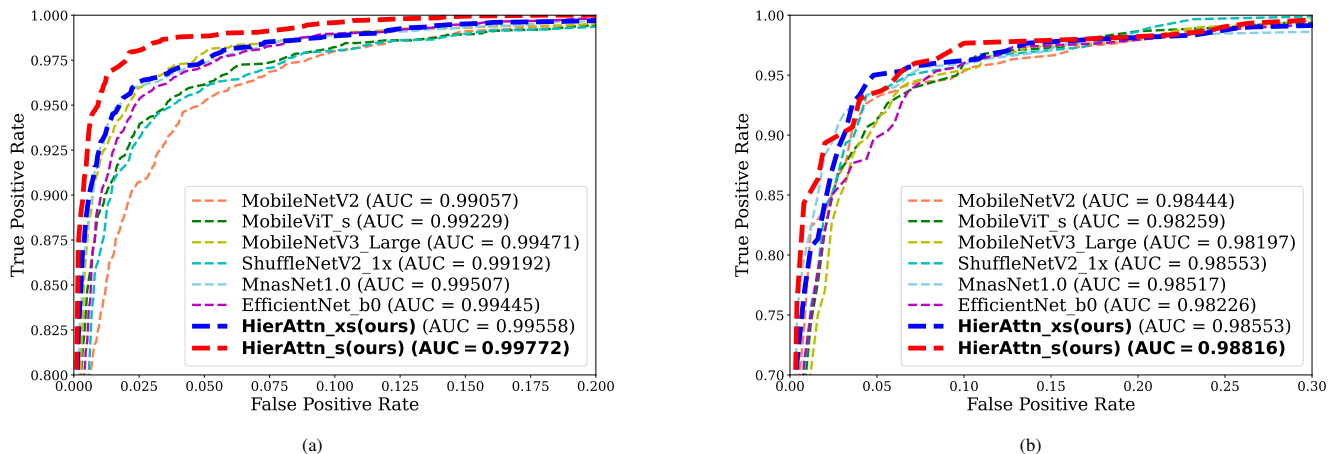


Fig. 8: ROC curves of different classification methods on skin lesions dataset (a) ISIC2019 validation set and (b) PAD2020 validation set.

and 0.7% accuracy than Rand in ISIC2019 and PAD2020, respectively. The diminishing improvement in the PAD dataset could be caused by the low imbalance ratio of PAD compared to the ISIC dataset (16.3 for PAD vs. 53.9 for ISIC). The effects of alleviating negative influence on classification are more obvious for the dataset with the higher imbalance ratio. Thirdly, the error bar of ISIC2019 is shorter than PAD2020, indicating that HierAttn is more robust on ISIC2019 than PAD2020.

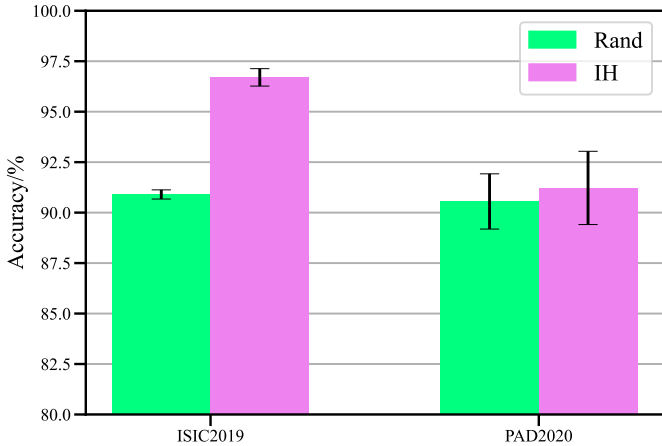


Fig. 9: Impact of different data balance methods.

4.3.3. Attention blocks in DWSCConv

Table 3 shows the number of parameters, inference time and accuracy of models using different attention mechanisms in DWSCConv. It can be discovered that without the attention mechanism [see Fig. 5 (a)], the network only achieved only 96.20% accuracy. However, HierAttn with SEAttn or SCAttn attains at least 0.45% more accuracy than without using the attention mechanism in DWSCConv. Although the accuracy of HierAttn with SCAttn is only 0.05% more than HierAttn with SEAttn, HierAttn with SCAttn is faster for inference (averaging 1000 iterations) with a smaller number of parameters than HierAttn with SEAttn.

Table 3: Impact of different attention mechanisms in DWSCConv.

Attention mechanism	# Parameters/M	Inference time/ms	Accuracy/%
-	2.14	1.551	96.20
SEAttn	2.17	1.663	96.65
SCAttn	2.14	1.658	96.70

4.3.4. Transfer learning warm-up

We consider that the models are unstable after partially transferring tunable parameters and randomly initialising those layers without transferring. Hence, we apply a warm-up technique to alleviate the influence of random weight initialisation for transferred layers. We freeze the transferred layers by stopping gradient backpropagation in the first 30 epochs. In these 30 epochs, only those layers without transferring can update their

parameters. Table 4 shows that the performance of the HierAttn_s with the transfer learning warm-up improves by 0.42% on the IHISIC2019 dataset.

4.3.5. Stochastic depth

Stochastic depth, also regarded as "layer dropout", is implemented in each layer with a skip connection in HierAttn. Typically, it is in all SCADW blocks with a stride of 1 and all CTH blocks. Table 4 demonstrates that the stochastic depth effectively enhances the performance of HierAttn_s by 0.65%. Note that even without this stochastic depth, the performance of HierAttn_s delivers similar or better results than SOTA mobile models.

4.3.6. Skip connection of CTH block

We add a skip connection link in the CTH (convolution-transformer hybrid) block with a stride of 1. Moreover, we also apply stochastic depth to those modules with skip connections. Thus, we can reuse the lower level feature and alleviate the gradient descent. Table 4 shows a 0.23% improvement in the performance of HierAttn_s with the skip connection. It demonstrates that stochastic depth can reduce the negative influence of adding two distinctive features in the skip connection of the CTH block.

Table 4: Impact on the accuracy under different ablation conditions.

Condition	Warm-up	Stochastic depth	Skip connection
Without	96.28	96.05	96.47
With	96.70	96.70	96.70

5. Discussion

From Table 3, we can also discover that even without attention after depthwise convolution, HierAttn still achieves the most considerable accuracy, 96.20%, than other SOTA lightweight models on the ISIC2019 validation set. It suggests that branch attention could be preferable to obtaining information on critical stages. It also shows a high potential to use branch attention as a general method for improving the performance of different models. Applying branch attention in a model with more layers, e.g., 300, can prevent the gradient descent in backpropagation.

Additional experiments were also conducted to investigate the inference time, and the results demonstrate that HierAttn_xs consumes lower than 1 ms for processing one image, 12% faster than MnasNet1.0's and just 9% slower than MobileNetV2's. Although the self-attention and branch attention mechanisms partially increase the network complexity, the HierAttn_xs model is still among the middle level in the inference time, with an acceptable sub-millisecond time cost for self-examination or clinical diagnosis.

We also proposed a larger version of HierAttn, HierAttn_m, with 5.44 M parameters. However, we have not trained or validated HierAttn_m due to limited computation resources. We

believe it also has appreciable potential to detect skin lesions in large hospitals or clinical centres that can support heavy computing in routine examinations.

Mobile application for skin cancer diagnosis allows dermatologists to perform point-of-care testing. Moreover, possible patients can carry out further detection by utilising mobile applications while doing regular self-exam. HierAttn has a statistically close speed to classic mobile networks, which shows great potential to be developed on mobile devices. If the skin lesion is recognised as MEL, BCC, ACK, SCC or VASC with more than 50% possibility, users are suggested to go to a clinic or hospital to perform further diagnosis. Otherwise, it is more likely that the detected area of the skin is healthy. We expect that HierAttn can be deployed on the mobile phone to assist ordinary people in performing regular self-check in the future.

6. Conclusion

In this paper, we propose a HierAttn network consisting of stage attention, branch attention, and SCAttn for skin lesions diagnosis. Stage attention consists of a SCADW block for downsizing feature maps and a CTH block for effectively learning the local and global representations. Branch attention applies hierarchical pooling after each stage attention to learn local and global representations and improve the feature interactions. SCAttn directly extracts global features by using only global average pooling without operating channel-wise information redundantly. With these novel modules, HierAttn can achieve better skin lesion classification results, 96.70% accuracy and 0.9972 AUC on ISIC2019 and 91.22% accuracy and 0.98816 AUC on PAD2020 validation set, than other SOTA mobile networks. Moreover, HierAttn is the smallest model among SOTA mobile networks, which shows great potential to be deployed in mobile devices for broader impacts on the general public.

Declaration of Competing Interest

The authors declare that they have no known competing financial interests or personal relationships that could have appeared to influence the work reported in this paper.

CRedit authorship contribution statement

Wei Dai: Conceptualization, Methodology, Validation, Writing. **Rui Liu:** Conceptualization, Methodology. **Tianyi Wu:** Conceptualization, Validation. **Min Wang:** Conceptualization. **Jianqin Yin:** Writing. **Jun Liu:** Conceptualization, Writing, Supervision.

Acknowledgments

This work was supported by the Research Grant Council (RGC) of Hong Kong under Grant 11212321 and Grant ECS-21212720, Guangdong Province Basic and Applied Basic Research Fund Project 2019A1515110175, and the Science and Technology Innovation Committee of Shenzhen under Grant Type-C 2022/86.

Supplementary Material

Supplementary material associated with this article can be found in the attachment file "Supplement.pdf".

References

- Adegun, A., Viriri, S., 2021. Deep learning techniques for skin lesion analysis and melanoma cancer detection: a survey of state-of-the-art. *Artificial Intelligence Review* 54, 811–841.
- Attique Khan, M., Sharif, M., Akram, T., Kadry, S., Hsu, C.H., 2021. A two-stream deep neural network-based intelligent system for complex skin cancer types classification. *International Journal of Intelligent Systems*.
- Avilés-Izquierdo, J.A., Molina-López, I., Rodríguez-Lomba, E., Marquez-Rodas, I., Suarez-Fernandez, R., Lazaro-Ochaita, P., 2016. Who detects melanoma? impact of detection patterns on characteristics and prognosis of patients with melanoma. *Journal of the American Academy of Dermatology* 75, 967–974.
- Buda, M., Maki, A., Mazurowski, M.A., 2018. A systematic study of the class imbalance problem in convolutional neural networks. *Neural Networks* 106, 249–259.
- Cassidy, B., Kendrick, C., Brodzicki, A., Jaworek-Korjakowska, J., Yap, M.H., 2022. Analysis of the isic image datasets: usage, benchmarks and recommendations. *Medical Image Analysis* 75, 102305.
- Celebi, M.E., Iyatomi, H., Schaefer, G., Stoecker, W.V., 2009. Lesion border detection in dermoscopy images. *Computerized Medical Imaging and Graphics* 33, 148–153.
- Chen, S., Wang, Z., Shi, J., Liu, B., Yu, N., 2018. A multi-task framework with feature passing module for skin lesion classification and segmentation, in: *IEEE 15th International Symposium on Biomedical Imaging (ISBI)*, IEEE. pp. 1126–1129.
- Combalia, M., Codella, N.C., Rotemberg, V., Helba, B., Vilaplana, V., Reiter, O., Carrera, C., Barreiro, A., Halpern, A.C., Puig, S., et al., 2019. Bcn20000: Dermoscopic lesions in the wild. *arXiv preprint arXiv:1908.02288*.
- Dai, D., Dong, C., Xu, S., Yan, Q., Li, Z., Zhang, C., Luo, N., 2022. Ms red: A novel multi-scale residual encoding and decoding network for skin lesion segmentation. *Medical Image Analysis* 75, 102293.
- Dosovitskiy, A., Beyer, L., Kolesnikov, A., Weissenborn, D., Zhai, X., Unterthiner, T., Dehghani, M., Minderer, M., Heigold, G., Gelly, S., et al., 2020. An image is worth 16x16 words: Transformers for image recognition at scale, in: *International Conference on Learning Representations*.
- Esteva, A., Kuprel, B., Novoa, R.A., Ko, J., Swetter, S.M., Blau, H.M., Thrun, S., 2017. Dermatologist-level classification of skin cancer with deep neural networks. *Nature* 542, 115–118.
- Gessert, N., Nielsen, M., Shaikh, M., Werner, R., Schlaefer, A., 2020. Skin lesion classification using ensembles of multi-resolution efficientnets with meta data. *MethodsX* 7, 100864.
- Guy Jr, G.P., Machlin, S.R., Ekwueme, D.U., Yabroff, K.R., 2015a. Prevalence and costs of skin cancer treatment in the us, 2002– 2006 and 2007– 2011. *American Journal of Preventive Medicine* 48, 183–187.
- Guy Jr, G.P., Thomas, C.C., Thompson, T., Watson, M., Massetti, G.M., Richardson, L.C., 2015b. Vital signs: melanoma incidence and mortality trends and projections—united states, 1982–2030. *MMWR. Morbidity and Mortality Weekly Report* 64, 591.
- He, X., Tan, E.L., Bi, H., Zhang, X., Zhao, S., Lei, B., 2022. Fully transformer network for skin lesion analysis. *Medical Image Analysis*, 102357.
- Hou, Q., Zhou, D., Feng, J., 2021. Coordinate attention for efficient mobile network design, in: *Proceedings of the IEEE/CVF Conference on Computer Vision and Pattern Recognition*, pp. 13713–13722.
- Howard, A., Sandler, M., Chu, G., Chen, L.C., Chen, B., Tan, M., Wang, W., Zhu, Y., Pang, R., Vasudevan, V., et al., 2019. Searching for mobilenetv3, in: *Proceedings of the IEEE/CVF International Conference on Computer Vision*, pp. 1314–1324.
- Howard, A.G., Zhu, M., Chen, B., Kalenichenko, D., Wang, W., Weyand, T., Andreetto, M., Adam, H., 2017. Mobilenets: Efficient convolutional neural networks for mobile vision applications. *arXiv preprint arXiv:1704.04861*.
- Hu, J., Shen, L., Sun, G., 2018. Squeeze-and-excitation networks, in: *Proceedings of the IEEE Conference on Computer Vision and Pattern Recognition*, pp. 7132–7141.
- Kawahara, J., Hamarneh, G., 2016. Multi-resolution-tract cnn with hybrid pre-trained and skin-lesion trained layers, in: *International Workshop on Machine Learning in Medical Imaging*, Springer. pp. 164–171.

- Lemaître, G., Nogueira, F., Aridas, C.K., 2017. Imbalanced-learn: A python toolbox to tackle the curse of imbalanced datasets in machine learning. *Journal of Machine Learning Research* 18, 559–563.
- Liu, Y., Lew, M.S., 2016. Learning relaxed deep supervision for better edge detection, in: *Proceedings of the IEEE conference on computer vision and pattern recognition*, pp. 231–240.
- Loeschner, L.J., Janda, M., Soyer, H.P., Shea, K., Curiel-Lewandrowski, C., 2013. Advances in skin cancer early detection and diagnosis, in: *Seminars in Oncology Nursing*, Elsevier. pp. 170–181.
- Loshchilov, I., Hutter, F., 2017. Sgdr: Stochastic gradient descent with warm restarts, in: *International Conference on Learning Representations*.
- Loshchilov, I., Hutter, F., 2018. Decoupled weight decay regularization, in: *International Conference on Learning Representations*.
- Mahbod, A., Schaefer, G., Wang, C., Dorffner, G., Ecker, R., Ellinger, I., 2020. Transfer learning using a multi-scale and multi-network ensemble for skin lesion classification. *Computer Methods and Programs in Biomedicine* 193, 105475.
- Mehta, S., Rastegari, M., 2021. Mobilevit: Light-weight, general-purpose, and mobile-friendly vision transformer, in: *International Conference on Learning Representations*.
- Pacheco, A.G., Lima, G.R., Salomão, A.S., Krohling, B., Biral, I.P., de Angelo, G.G., Alves Jr, F.C., Esgario, J.G., Simora, A.C., Castro, P.B., et al., 2020. Pad-ufes-20: a skin lesion dataset composed of patient data and clinical images collected from smartphones. *Data in Brief* 32, 106221.
- Pan, J., Bulat, A., Tan, F., Zhu, X., Dudziak, L., Li, H., Tzimiropoulos, G., Martinez, B., 2022. Edgevits: Competing light-weight cnns on mobile devices with vision transformers. *arXiv preprint arXiv:2205.03436*.
- Peruch, F., Bogo, F., Bonazza, M., Cappelleri, V.M., Peserico, E., 2013. Simpler, faster, more accurate melanocytic lesion segmentation through meds. *IEEE Transactions on Biomedical Engineering* 61, 557–565.
- Reiß, S., Seibold, C., Freytag, A., Rodner, E., Stiefelwagen, R., 2021. Every annotation counts: Multi-label deep supervision for medical image segmentation, in: *Proceedings of the IEEE/CVF Conference on Computer Vision and Pattern Recognition*, pp. 9532–9542.
- Sandler, M., Howard, A., Zhu, M., Zhmoginov, A., Chen, L.C., 2018. Mobilenetv2: Inverted residuals and linear bottlenecks, in: *Proceedings of the IEEE Conference on Computer Vision and Pattern Recognition*, pp. 4510–4520.
- Smith, M.R., Martinez, T., Giraud-Carrier, C., 2014. An instance level analysis of data complexity. *Machine Learning* 95, 225–256.
- Song, J., Chen, Y., Ye, J., Song, M., 2022. Spot-adaptive knowledge distillation. *IEEE Transactions on Image Processing*.
- Sung, H., Ferlay, J., Siegel, R.L., Laversanne, M., Soerjomataram, I., Jemal, A., Bray, F., 2021. Global cancer statistics 2020: Globocan estimates of incidence and mortality worldwide for 36 cancers in 185 countries. *CA: a Cancer Journal for Clinicians* 71, 209–249.
- Suwanwimolkul, S., Komorita, S., 2022. Efficient linear attention for fast and accurate keypoint matching. *arXiv preprint arXiv:2204.07731*.
- Szegedy, C., Liu, W., Jia, Y., Sermanet, P., Reed, S., Anguelov, D., Erhan, D., Vanhoucke, V., Rabinovich, A., 2015. Going deeper with convolutions, in: *Proceedings of the IEEE Conference on Computer Vision and Pattern Recognition*, pp. 1–9.
- Tan, M., Chen, B., Pang, R., Vasudevan, V., Sandler, M., Howard, A., Le, Q.V., 2019. Mnasnet: Platform-aware neural architecture search for mobile, in: *Proceedings of the IEEE/CVF Conference on Computer Vision and Pattern Recognition*, pp. 2820–2828.
- Tan, M., Le, Q., 2019. Efficientnet: Rethinking model scaling for convolutional neural networks, in: *International Conference on Machine Learning*, PMLR. pp. 6105–6114.
- Tang, P., Liang, Q., Yan, X., Xiang, S., Zhang, D., 2020. Gp-cnn-dtel: Global-part cnn model with data-transformed ensemble learning for skin lesion classification. *IEEE Journal of Biomedical and Health Informatics* 24, 2870–2882.
- Tang, P., Yan, X., Nan, Y., Xiang, S., Krammer, S., Lasser, T., 2022. Fusionm4net: A multi-stage multi-modal learning algorithm for multi-label skin lesion classification. *Medical Image Analysis* 76, 102307.
- Tschandl, P., Rosendahl, C., Kittler, H., 2018. The ham10000 dataset, a large collection of multi-source dermatoscopic images of common pigmented skin lesions. *Scientific Data* 5, 1–9.
- Wang, L., Lee, C.Y., Tu, Z., Lazebnik, S., 2015. Training deeper convolutional networks with deep supervision. *arXiv preprint arXiv:1505.02496*.
- Weng, W.H., Deaton, J., Natarajan, V., Elsayed, G.F., Liu, Y., 2020. Addressing the real-world class imbalance problem in dermatology, in: *Machine Learning for Health*, PMLR. pp. 415–429.
- Woo, S., Park, J., Lee, J.Y., Kweon, I.S., 2018. Cbam: Convolutional block attention module, in: *Proceedings of the European Conference on Computer Vision (ECCV)*, pp. 3–19.
- Wu, H., Chen, S., Chen, G., Wang, W., Lei, B., Wen, Z., 2022. Fat-net: Feature adaptive transformers for automated skin lesion segmentation. *Medical Image Analysis* 76, 102327.
- Xie, Y., Zhang, J., Xia, Y., Shen, C., 2020. A mutual bootstrapping model for automated skin lesion segmentation and classification. *IEEE Transactions on Medical Imaging* 39, 2482–2493.
- Yang, C., Wang, Y., Zhang, J., Zhang, H., Wei, Z., Lin, Z., Yuille, A., 2022. Lite vision transformer with enhanced self-attention, in: *Proceedings of the IEEE/CVF Conference on Computer Vision and Pattern Recognition*, pp. 11998–12008.
- Zhang, L., Chen, X., Zhang, J., Dong, R., Ma, K., 2022. Contrastive deep supervision. *arXiv preprint arXiv:2207.05306*.
- Zhang, X., Zhou, X., Lin, M., Sun, J., 2018. Shufflenet: An extremely efficient convolutional neural network for mobile devices, in: *Proceedings of the IEEE Conference on Computer Vision and Pattern Recognition*, pp. 6848–6856.
- Zhou, H., Schaefer, G., Celebi, M.E., Lin, F., Liu, T., 2011. Gradient vector flow with mean shift for skin lesion segmentation. *Computerized Medical Imaging and Graphics* 35, 121–127.